Imaging properties of the Gabor superlens

1999 J. Opt. A: Pure Appl. Opt. 1 94

(http://iopscience.iop.org/1464-4258/1/1/013)

J. Opt. A: Pure Appl. Opt. **1** (1999) 94–102. Printed in the UK PII: S1464-4258(99)97245-8

Imaging properties of the Gabor superlens

C Hembd-Sölner, R F Stevens and M C Hutley

National Physical Laboratory, Centre for Length Metrology, Queens Road, Teddington, Middlesex TW11 0LW, UK

Received 7 September 1998

Abstract. A superlens is an optical system consisting of a pair of microlens arrays in which there is a slight difference in pitch. The relative displacement of one lens with respect to its partner causes the bundle of light passing through a pair of lenses to be deviated in such a way that all bundles converge to a common point and the system behaves like a lens. The focal properties are very different from those of a conventional lens and were originally described by Gabor in 1940. We have extended his analysis and have taken advantage of modern technology to assemble superlenses and confirm their properties experimentally.

Keywords: Lens arrays, microlenses, optical imaging, superlens

1. Introduction

In 1940 Gabor described an optical system consisting of a pair of arrays of microlenses [1]. The arrays were separated by the sum of their focal lengths and there was a small difference between the periods of the two arrays. The overall effect was to perform a function similar to that of a lens with dimensions much larger than the microlenses in the arrays. Images formed by this system exhibit unusual properties and appear not to obey the normal rules of optics, for example, the magnification is not necessarily equal to the ratio of image to object distances. Gabor assigned the term 'superlens' to the system.

He initially considered arrays of cylindrical lenses as they were readily available but pointed out that arrays of spherical lenses could be combined to form superlenses. The lenses were aligned in such a way that they formed an array of miniature telescopes. Because of the difference in period each lens was, in general, displaced sideways with respect to its partner in the other array. A beam of light entering a telescope would be deviated by an angle that depended upon the focal lengths of the lenses and their relative displacement. As the displacement varied progressively across the array so the deviation varied in such a way that a collimated incident beam would be divided into an array of smaller beams which would converge to a common point or position of minimum confusion. The combination would therefore perform a function similar to that of a lens.

The difference in period between the lens arrays is responsible for the relative displacement of the lenses and also for the number of points at which alignment of the lenses occurs. Thus a pair of lens arrays can produce the effect of an array of larger lenses and it was these that Gabor termed 'superlenses'. He coined the term after consideration of the term 'superlattice', used in crystallography. The superlenses do not have discrete boundaries but their apertures merge into one another. It is therefore possible to produce multiple images of the same object using a superlens array. In this paper we consider just one of those 'superlenses'.

There is a special case of the superlens in which the two lens arrays have the same period and focal length. Such a system will form an erect image of unit magnification and it is possible to form an image of a large area with a very small distance between the object and the image. Equal-period systems are commonly found in photocopiers and facsimile machines. These were studied in some detail by Anderson [2] who made close-up imaging systems for oscilloscope cameras. These days, lens array systems are usually formed as linear arrays of graded-index rod lenses [3], but they have also been made with independent arrays of microlenses. The analysis in this paper may therefore be regarded as a generalization of this common optical system. The system is also related to that of the moiré magnifier [4] in which the moiré pattern formed between a lens array and an array of objects gives a magnified image of the object. In this case we have Vernier moiré fringes and the array of images formed by the first array serves as the array of objects for the second lens array.

The purpose of this paper is to extend Gabor's analysis. We are also able to take advantage of recent developments in the technology of the manufacture of arrays of spherical microlenses and to put together superlenses to confirm their properties experimentally. As far as we are aware this is the first practical demonstration of the device†.

† We note that Anderson introduced demagnification in his system by using arrays of different period but under conditions which were different from the operation of a true superlens

1464-4258/99/010094+09$19.50

2. Paraxial imaging equation

The principle of the superlens is illustrated in figure 1. A collimated incident beam is divided into a series of smaller beams which are steered by miniature telescopes towards a common 'focus'. An image formed by the intersection of bundles of rays is known as an 'integral' image following the terminology of Lippmann with his integral photography [5]. It is interesting to note that although the optical paths within the individual bundles are constrained by Fermat's principle, the formation of the integral image is not.

The diagram shows a superlens consisting of arrays of positive lenses which form Keplerian telescopes.

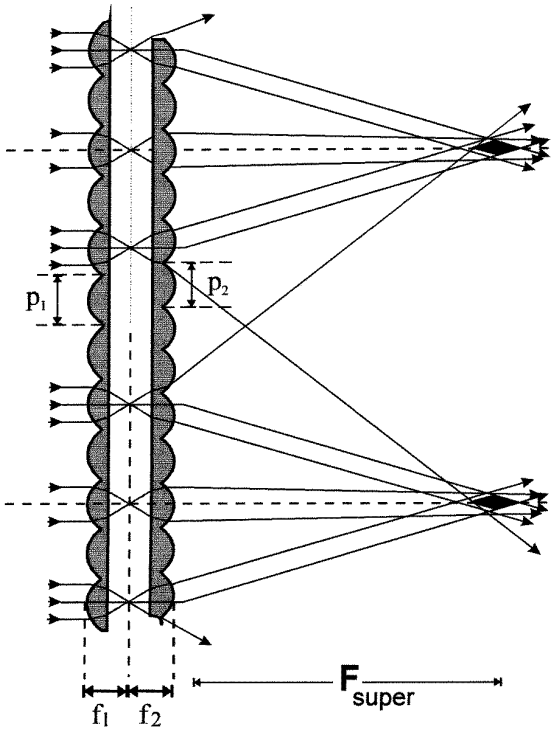

Figure 1. Focusing of rays by a superlens.

Alternatively one could use an array of positive lenses in conjunction with an array of negative lenses to form Galilean telescopes. Both systems are governed by the same equations but the Kepler type exhibits properties which are strikingly different from those of a conventional lens.

We will consider far-field imaging first, where the rays emerging from an object point are considered as parallel bundles of rays that are deviated and leave as parallel bundles [6]. Even for small imaging distances this may be a good approximation, if the microlenses are small and the diffraction-limited spot size is of the order of the microlens diameter. On the other hand, it is necessary to adjust the spacing between the microlens arrays and refocus the beams in the integral image plane, if close-up imaging with high resolution needs to be achieved.

2.1. Far-field imaging

Consider a parallel bundle of rays incident at an angle α in figure 2. These will be brought to a focus at a point P, a distance $f_1\alpha$ from the axis of the first lens. The second lens will then collimate the light diverging from P and it will emerge at an angle β given by

$$\beta = \frac{f_1\alpha - \Delta}{f_2} \tag{1}$$

where Δ is the displacement between the optical axes of the first and second lenses.

Now consider a bundle of rays from a source a distance u from the lens arrays, incident at a radial position r as shown in figure 3. The bundle will emerge at an angle β and its lateral position at a distance x from the lens arrays is given by

$$y = r - \beta x. \tag{2}$$

If we now set $\alpha = r/u$ and substitute for β from equation (1) we have

$$y = r - \frac{x}{f_2}\left[\frac{r}{u}f_1 - \Delta_r\right] = r\left[1 - \frac{xf_1}{uf_2}\right] + \frac{x\Delta_r}{f_2} \tag{3}$$

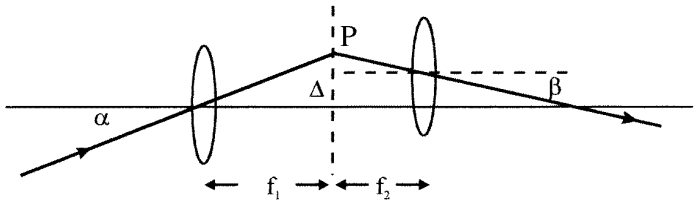

Figure 2. Deviation of rays by a telescope with decentred lenses.

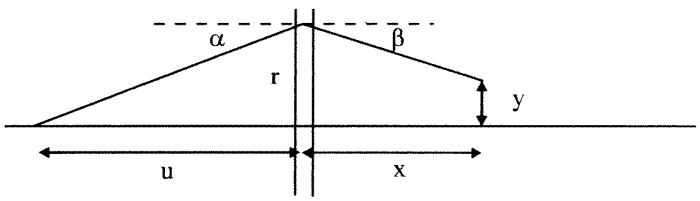

Figure 3. Deviation of parallel bundles in a superlens.

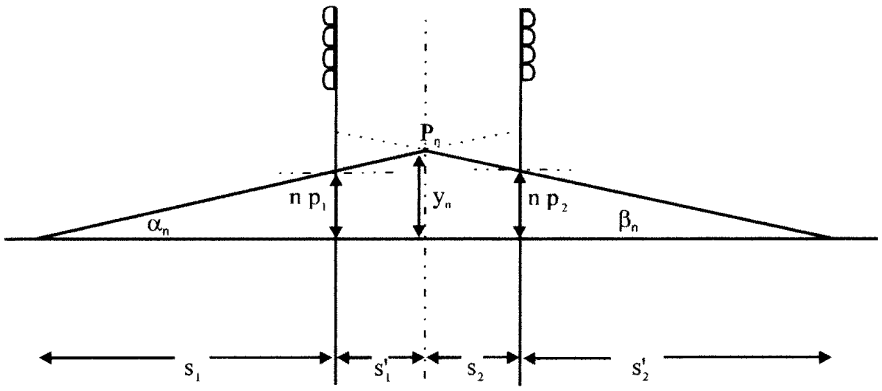

Figure 4. Paraxial imaging by two lens arrays.

where Δ_r is the relative displacement of the lenses at a distance r from the axis.

The condition for a focus is that bundles passing through all regions of the lens array should meet at the same point, i.e. the value of y is independent of r so $\partial y/\partial r = 0$. If we differentiate and rearrange equation (3) and set $x = v$, the image distance, we obtain the result

$$\frac{1}{v} = \frac{f_1}{f_2}\frac{1}{u} + \frac{1}{f_2}\frac{\partial \Delta_r}{\partial r}. \tag{4}$$

This bears some resemblance to the simple lens formula and we may find the focal length F of the array by setting $u = \infty$ and $v = F$. We obtain

$$F = \frac{f_2}{\partial \Delta_r/\partial r}. \tag{5}$$

This analysis indicates that when there is a constant difference in period between the two arrays the combination will form an integral image. It does so in a manner similar to that of a simple lens in which the focal length is a function of the focal length of the collimating microlenses and the proportional difference in period. It is, however, only a first approximation even to the paraxial case, because the focal lengths of the microlenses have been considered small compared to the image and object distances.

2.2. General case

In a more refined description we take account of the fact that the lenses of the first array form images of the object at the intermediate plane and that the lenses of the second array re-image these into the final image. Within this condition there are two ways in which the lens can be used. If we adjust the separation of the lenses to give the best possible image for a particular image and object plane we may either adjust that separation for other conjugates or we may keep it fixed. In the first case the superlens is active and the analysis is appropriate to one set of conjugates. In the second case the superlens is passive and the analysis is appropriate to the imaging of objects of finite depth.

We consider first the active case for which the relevant parameters are shown in figure 4. A point on the optical axis is imaged by the first lens array of pitch p_1 to a set of points P_n a distance s_1' behind the first lens array as depicted in figure 4. We use the sign convention where distances to the left of a refracting surface like s_1 and s_2 are negative. In the drawing we consider the chief ray of the *n*th pair of microlenses. P_n is imaged by the second lens array a distance s_2' behind the second lens array. In order to have this point lying on the optical axis of the superlens the image height should be zero. We can state this in the form

$$y_n - \beta_n(s_2' - s_2) = 0. \tag{6}$$

Now $y_n = \alpha_n(s_1 - s_1')$ and $\alpha_n = np_1/s_1$, while $\beta_n = n\ p_2/s_2'$ and therefore equation (6) becomes

$$np_1\frac{s_1 - s_1'}{s_1} = np_2\frac{s_2' - s_2}{s_2'}. \tag{7}$$

The fact that equation (7) is independent of *n* indicates that all beams can be focused to the same spot by adjusting the separation of the lens arrays. However, it should be borne in mind that this can only be achieved for one plane at a time. The equation still holds in the case of pairs of positive and negative lenses forming arrays of Galilean telescopes.

In order to eliminate s_1' and s_2, we use the thin lens equation

$$\frac{1}{s_1'} = \frac{1}{s_1} + \frac{1}{f_1'} \qquad \text{or} \qquad s_1' = \frac{s_1 f_1'}{s_1 + f_1'}. \tag{8}$$

This leads to

$$(p_1 - p_2) = p_1\frac{f_1'}{f_1' + s_1} + p_2\frac{f_2'}{s_2' - f_2'}. \tag{9}$$

In the limit where $s_1 \to \infty$, s_2' becomes the back focal length F_{super} of the superlens,

$$F'_{\text{super}} = f_2'\frac{p_1}{(p_2 - p_1)}. \tag{10}$$

If, on the other hand, light is incident from the other direction we have

$$F_{\text{super}} = f_1\frac{p_2}{(p_1 - p_2)}. \tag{11}$$

These are equivalent to equations (4) and (5). If we divide equation (9) by $p_1 f_2'$ and use the expression (10) for the focal length F' we obtain

$$\frac{1}{F'_{\text{super}}} = \frac{f_1'}{f_2'}\frac{1}{(f_1' + s_1)} + \frac{p_2}{p_1}\frac{1}{(s_2' - f_2')} \tag{12}$$

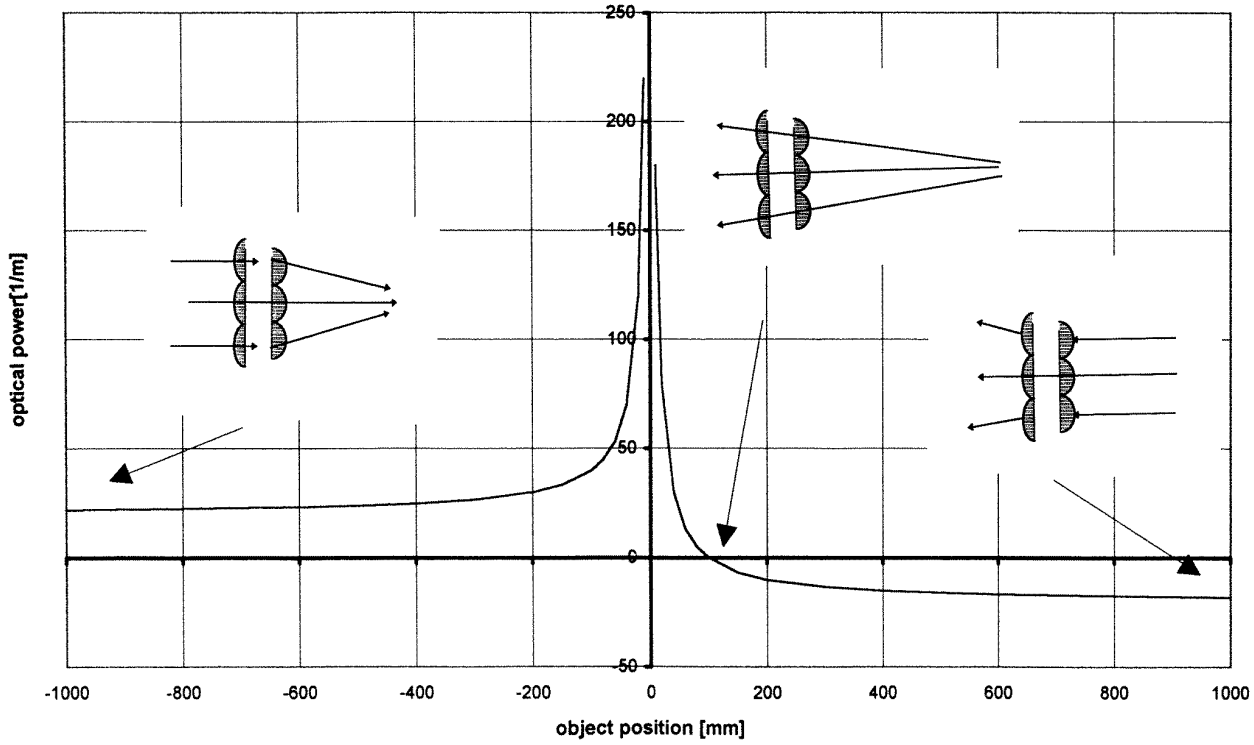

Figure 5. Optical power of a superlens.

which reduces to equation (4) in the limit where $f_1 \ll s_1$ and $f_2 \ll s_2$.

Equation (12) is the basic equation for the superlens. It bears some resemblance to the equation of a normal lens in which $(f_1' + s_1)$ and $(s_2' - f_2')$ are the object and image distances, respectively. These are measured from planes situated outside the superlens at distances equal to the focal length of the microlenses.

2.3. Passive mode

In order to produce the best image of an object of finite depth the separation of the lens arrays should be determined by the best focus of a plane within the object. For points outside this plane we cannot expect a point image even within the paraxial approximation. Instead, we get an area of intersection of defocused bundles. We can restate equation (12) in a slightly different way to describe this. Starting with equation (7) we set s_1 and s_2' at the correct distance for the best image plane. Rearranging and using the expression (10) for the focal length of the superlens as before, this leads to

$$\frac{1}{F'_{\text{super}}} = \frac{s_1'}{f_2'}\frac{1}{s_1} - \frac{p_2}{p_1}\frac{s_2}{f_2'}\frac{1}{s_2'}. \tag{13}$$

For the case of a typical superlens the design conjugates are at infinity, $s_1' = f_1'$ and $s_2 = f_2 = -f_2'$ and we recover equation (4) in a slightly different form,

$$\frac{1}{F'_{\text{super}}} = \frac{f_1'}{f_2'}\frac{1}{s_1} + \frac{p_2}{p_1}\frac{1}{s_2'}. \tag{14}$$

The difference from equation (12) is due to the fact that (14) describes imaging at different conjugates while keeping the separation fixed, as with a cemented component.

2.4. Interpretation and characteristic features

We can approach the analysis in two ways. On the one hand we can define the optical power of the superlens as the optical power of a corresponding thin lens which relates the image and object distances by the simple lens equation. If we rearrange equation (4) this leads to the conclusion that the 'optical power' is a function of the object distance,

$$\frac{1}{v} + \frac{1}{u} = \frac{1}{u}\left[\frac{f_1}{f_2} + 1\right] + \frac{1}{F'_{\text{super}}}. \tag{15}$$

Alternatively one can define the focal length in terms of the distance between the integral image and the superlens when illuminated with collimated light. This is what we have done in the analysis and it leads to an imaging equation which resembles but is not the same as that of a conventional lens. In Gabor's analysis he described the focal properties as though the image were formed in a medium of refractive index which depended upon the conjugates.

The first approach has the advantage that we are able to associate with the superlens an 'optical power' which is given by the right-hand side of equation (15) and which we plot in figure 5 for a Kepler-type superlens. It varies from positive to negative as the object distance varies between plus and minus infinity and has a value of zero when the object lies at the point of intersection of the optical axes of the micro-telescopes.

These results are counterintuitive if one regards the superlens as a single component. It is surprising to see, as we shall show in figure 11, a magnified image when one looks through it in one direction and a diminished image when it is reversed. On the other hand, if we acknowledge that the superlens is an optical system, we avoid misleading

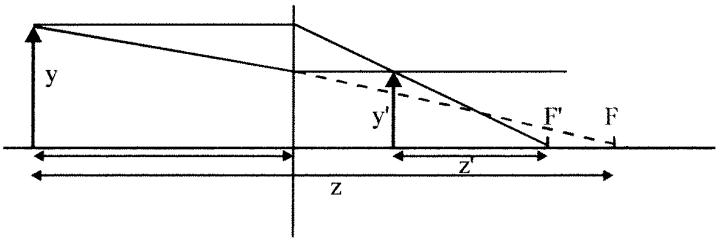

Figure 6. Geometrical image construction for a superlens.

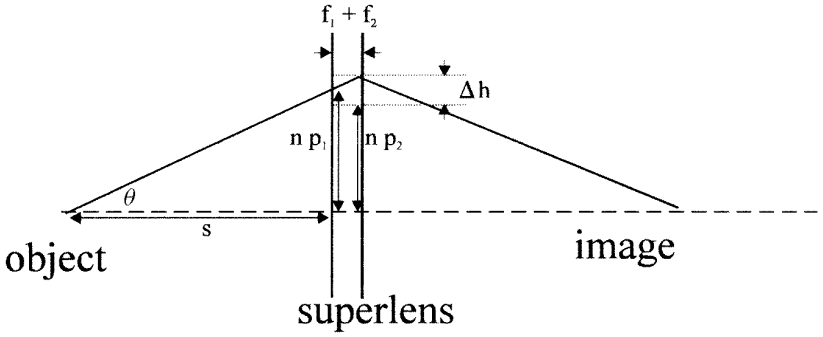

Figure 7. Limits of aperture of a superlens.

preconceptions. (We are familiar with the fact that a telescope used in reverse behaves differently.)

With this in mind we note the following features which contrast with normal lenses.

For the Kepler configuration:

- A negative superlens forms a real image for object distances s with $|s| < F_s f_1/f_2$.
- The image distance s' is always smaller than F_s' for a positive lens $F_s' > 0$.
- The superlens forms an erect image.
- For arrays of equal pitch the focal properties are the same as those of a plane mirror. For those of unequal pitch they resemble those of a spherical mirror.

For the Galilean configuration

- The lens behaves like a conventional lens in that the sign of F_s' does not change when the lens is turned round, but the focal length will, in general, depend on the orientation.
- It behaves like a conventional lens in which the object is immersed in a medium of refractive index f_1/f_2.

2.5. Image construction and magnification

In considering the magnification a better physical insight is obtained by using a simplified analysis. The geometrical image construction is shown in figure 6 when the position of the image is determined by the intersection of two bundles of rays. One ray from the object travelling parallel to the axis will be directed towards the positive focal point F'. A ray travelling towards the negative focal point F will be redirected parallel to the axis. From which it may be seen that

$$\frac{y}{y'} = \frac{F'}{z'} = \frac{z}{F} \tag{16}$$

and Newton's formula holds. The lateral magnification m_{lateral} is given by

$$m_{\text{lateral}} = 1 - \frac{s'}{F_s} \tag{17}$$

while the axial magnification is given by

$$m_{\text{axial}} = \frac{f_1}{f_2} m_{\text{lateral}}^2. \tag{18}$$

For a positive superlens ($F_s' > 0$) of the Kepler type the axial magnification is always smaller than unity and in the case of a negative superlens the magnification is always greater than unity.

2.6. Aperture

Given a specific pitch p and pitch difference dp of the superlens the relative shift of the lens arrays repeats after $p/\Delta p$ lenses. In fact each superlens is always part of an array of superlenses. At any point except on the axis, the light which is focused by a microlens in the first array is shared between adjacent microlenses in the second array by an amount that depends upon the relative displacement of those lenses. The superlenses have no sharp aperture but overlap, with the efficiency of each decreasing towards the edge. However, in practice it is useful to define the superlens diameter and to relate it to the period of the moiré pattern, $p^2/\mathrm{d}p$.

For the Kepler configuration the effective aperture of the system decreases as the object approaches. This is because as the angle of incidence at the peripheral microlenses increases, the proportion of light collected by its partner decreases. We can quantify this effect as follows.

$$\Delta h = n\Delta p + (f_1 + f_2)\theta. \tag{19}$$

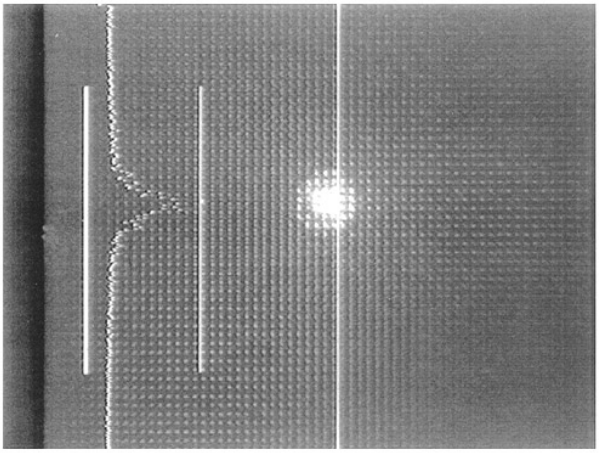

Figure 8. Focal spot of a superlens with a focal length of 64 mm.

Consider a point at image distance s as in figure 7. For the chief ray of the nth microlens, for this to be the marginal ray of the superlens we set

$$\Delta h \leqslant p/2. \tag{20}$$

Therefore we have

$$\tan\theta \leqslant \frac{p/2}{f_1 + f_2 + s\Delta p/p} \tag{21}$$

or in terms of the lens diameter $d = 2\tan(\theta)s$,

$$d = \frac{ps}{f_1 + f_2 + s\Delta p/p}. \tag{22}$$

3. Experimental confirmation of paraxial properties

3.1. Imaging equation

The experimental verification of the paraxial equation was carried out using the following pairs of arrays of lenses.

(a) Positive lenses with pitches of 253 and 250 μm (the Kepler configuration). Focal lengths of the lenses in both arrays 775 μm. The period of the moiré pattern between the arrays was approximately 20 mm, which was the maximum aperture of the superlens.
(b) Positive lenses with pitches of 253 and 251.5 μm, focal lengths of 500 and 625 μm and a moiré period of 43 mm.
(c) Positive and negative lens arrays (Galileo configuration) with pitches of 253 and 250 μm and focal lengths of 440 and -850 μm.

The lenses were formed according to the now common technique of melting small cylinders of photoresist [7] on good-quality optical substrates. Negative lenses were formed by casting the photoresist lens arrays into resin. On some examples interstitial masks were applied to prevent the transmission of light through the areas between the lenses. These were not, however, needed for the confirmation of the imaging equation and, in fact, they made relatively little difference to the quality of the image. We attribute this to the fact that most of the light passing through the interstices of the first array is collected by the lenses of the second array and dispersed over a wide range of angles.

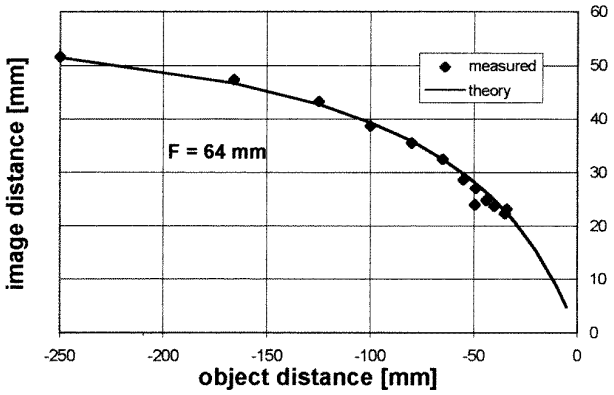

Figure 9. Experimental investigation of image equation (12) for a superlens.

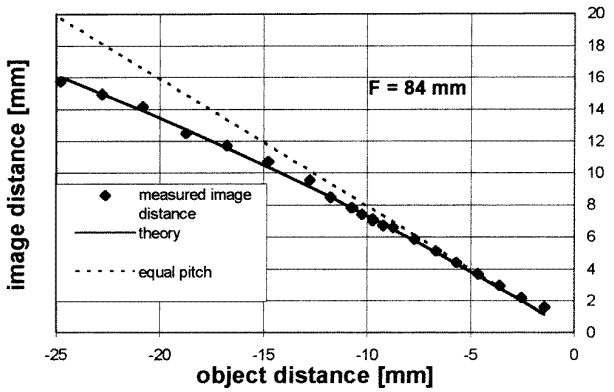

Figure 10. Experimental investigation of image equation (12) for a superlens ($F_s' = 84$ mm) at short object distances.

For the experiments described here the lens arrays were mounted separately but subsequently they were cemented together with appropriate spacers to provide a single component. In principle it should be possible to generate the two lens arrays on opposite sides of a common substrate to provide a monolithic device. However, in the present case one array was mounted on a mechanical stage which provided precise adjustment in three orthogonal linear directions and the other on a stage which provided rotational adjustment about three orthogonal axes. The initial adjustment was carried out by visually setting the moiré pattern to the maximum period. Thereafter the lenses were illuminated with a collimated laser beam and adjusted until the beam that emerged was focused to a minimum spot size and undeviated.

For superlens (a) the focal length was calculated to be 63.25 mm and the measured value was 64 ± 0.5 mm. The diameter of the focal spot was 0.5 mm which was double the diameter of the individual lenses. The size of the spot is influenced by the following factors.

- Diffraction at the aperture of the lenses (expected spread of 200 μm).
- Aberrations of the individual microlenses. For each pair of lenses the second lens generates a magnified image of the focal spot generated by the first lens. This effect will be exacerbated off-axis.

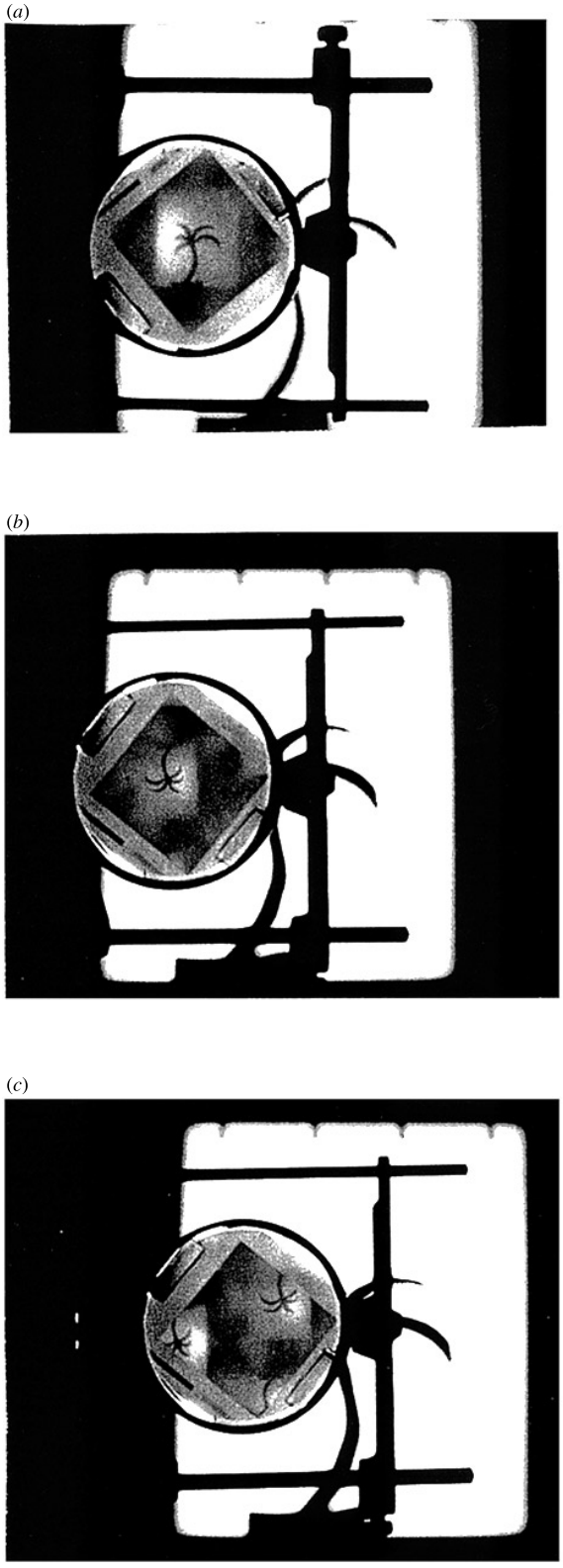

Figure 11. (*a*) Real image formed by positive superlens, (*b*) virtual image formed by negative superlens and (*c*) multiple images formed by negative superlens.

- Variations in the focal length of the microlenses result in out of focus images being formed at the plane of the integral image.

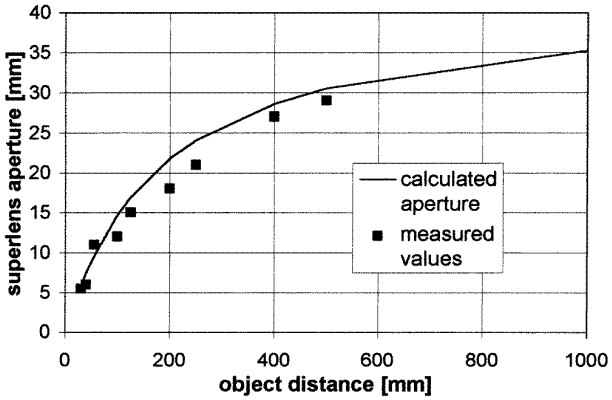

Figure 12. Aperture of a superlens as a function of object distance.

Figure 8 shows the focus of a superlens. The fine structure corresponds to the diffraction pattern of the lens array as it appears in coherent light. The period of the raster pattern is 200 μm $\times$ 200 μm.

In order to test the image equation, a point object was generated by focusing the light in front of the superlens at various distances. The corresponding image distance was measured for a variety of points. The graph of the image distance as a function of the object distance is shown in figures 9 and 10 and compared to the theoretically expected values from equation (12), calculated for a focal length of 64 mm. From this we see that equation (12) is confirmed. For large object and image distances as shown in figure 9 it was sufficient to measure the distances with a ruler. For shorter object distances a more precise experiment was conducted in which the modulation transfer function was measured and displayed in real time and used to determine the position of best focus. For large image distances the separation of the lens arrays remained constant, but in the more precise measurements of figure 9 the separation was adjusted to give the best focus. Numerical calculations with ray tracing were also performed and confirmed that the equation is valid for object distances as small as 20 mm.

To show the difference in the imaging behaviour of the Kepler-type superlens in two different directions we photographed an object through a superlens, which in this case was a cemented pair of lens arrays. The height of the object was 270 mm and the distance between the object and the superlens was 2 m. Figure 11(*a*) shows a real image which is upright as can be seen by comparison with the object.

Reversing the superlens gives a negative lens which produces a virtual inverted image as in figure 11(*b*). Depending on the camera position multiple images can be seen as in figure 11(*c*). We tested a Galilean-type superlens as well and confirmed that it gives an inverted real image like any conventional lens but the magnification depends on the orientation of the superlens.

3.2. Measurement of aperture

According to equation (22) the aperture of the superlens depends strongly on the object distance. To confirm this a superlens with diameter 45 mm was used. The pitches of the lens arrays were 253 and 251.5 μm, with focal lengths

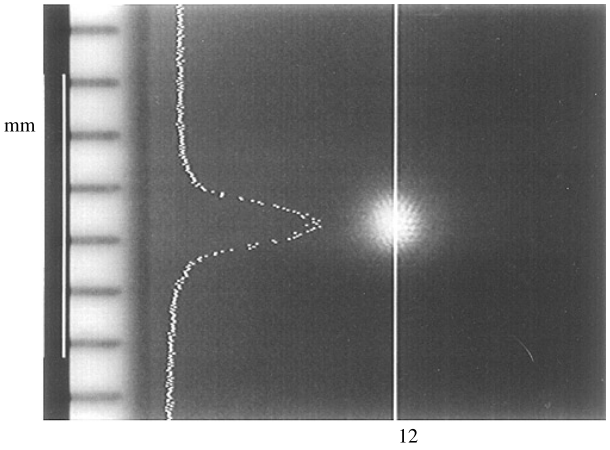

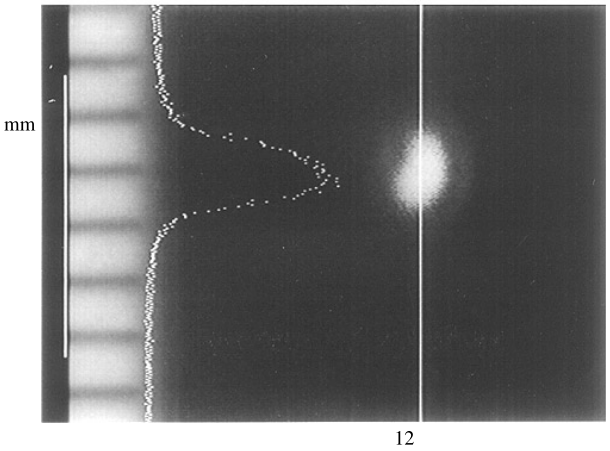

Figure 13. Point images on axis and 10° off-axis.

of 610 and 500 μm, respectively. Equation (22) gives an aperture of $p^2/\mathrm{d}p = 42$ mm in a parallel beam. A point on the optical axis was imaged and an iris was put in front of the superlens. The intensity in the image point was measured by a photodiode as a function of the stop diameter. As a practical approximation for the lens diameter we took the value of iris diameter which admits 50% of the intensity in the image point. Figure 12 shows the measured values of beam diameter as a function of object distance and compares them with the theoretical values from equation (22). For small object distances the aperture is

$$ps/(f_1 + f_2)$$

i.e. proportional to the object distance and independent of the pitch difference. For close-up imaging a positive superlens behaves like an afocal pair of lens arrays of equal pitch.

4. Nonparaxial properties

Away from the paraxial condition, light passes through the microlenses at a significant angle. This introduces aberrations both in the images formed by the lenses in the first array and in their re-imaging by the second one. The individual images are degraded and so in turn is the integral image. Furthermore, because of the field curvature of the

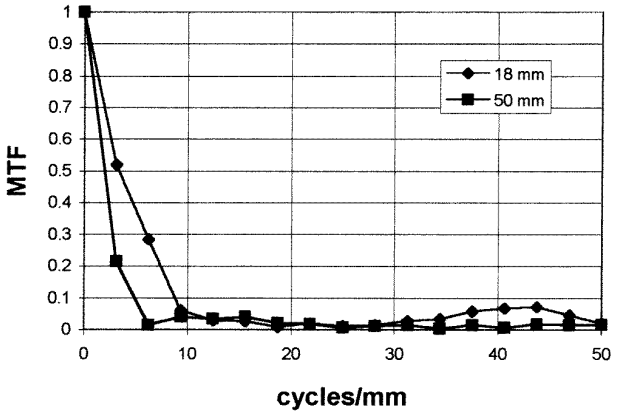

Figure 14. MTF for 18 and 50 mm object distances.

lenses of the first array the intermediate image is formed closer to the first array than in the paraxial case. This has two effects. First, the intermediate image is displaced radially so the deviation of the beam is less than that predicted by the simple theory. This has an effect which is similar to spherical aberration in a conventional lens. Second, the second lens is too far away from the first to focus the light onto the plane of the integral image and in order to obtain the best result it is necessary to reduce the separation of the lens arrays.

It has been observed that when a system is set up for collimated incident light it is necessary to move the lens arrays closer together to obtain the best image of a source at a finite distance. This is counter to intuitive expectations because as the source moves closer to the lenses in the first array, the intermediate image distance increases and one would expect to have to increase the separation of the arrays. We postulate that most of the energy in the image comes via a non-paraxial path and that the effect of field curvature dominates over that of the shift of the intermediate image.

The paraxial theory as given above cannot predict the spot size of the superlens. The shape of the individual beams which form the integral image is determined by the shape of the intermediate images formed by the lenses of the first array. These will be distorted through astigmatism and coma as one goes away from the axis. These images are then re-imaged by the lenses of the second array, which will themselves be working off-axis, and enlarged by a factor of $p/\mathrm{d}p$ when projected to the plane of the integral image. It is clear from figure 13 that off-axis imaging properties are significantly inferior to those on axis.

Finally, figure 14 shows an MTF measurement of a superlens for a point on axis for two different axial distances. The MTF performance improves for small object distances because it is less limited by diffraction at the apertures of the microlenses. Nevertheless, the performance is still significantly inferior to a conventional lens.

5. Conclusions

In his original work Gabor presented a very thorough and detailed analysis of the superlens but he did not have the means to verify it experimentally. His analysis was confined to the Galilean system and to the case where the lenses

were separated by the sum of their focal lengths. We have derived some of Gabor's results in a different way, have considered both Keplerian and Galilean configurations and have considered the case where the separation of the lens arrays is adjusted to focus each beam at the plane of the integral image.

We have also manufactured superlenses, studied their optical properties experimentally and confirmed the theoretical analysis within the limits of uncertainty imposed by the properties of the lens arrays.

At present we regard the superlens as an optical system with interesting optical properties but with image-forming capabilities of fairly limited application. However, we have noted that a degenerate form of superlens, that with arrays of equal pitch, is widely used in office copiers and is under serious consideration for microlithographic applications [8]. Extensions of this based on non-parallel arrays of graded index rod lenses have already been proposed [9]. Furthermore, significant progress is being made in the production of better-quality lens arrays of increased sophistication. We therefore suggest that it is possible that further practical applications for the superlens will be found and put into practice. We hope that the present work will contribute to that process.

References

[1] Gabor D 1940 *UK Patent* 541 753
[2] Anderson R H 1979 Close-up imaging of documents and displays with lens arrays *Appl. Opt.* **18** 477–84
[3] Rees J D 1982 Non-Gaussian imaging properties of GRIN fiber lens arrays *Appl. Opt.* **21** 1009–12
[4] Hutley M C, Hunt R and Stevens R F 1994 The moiré magnifier *Pure Appl. Opt.* **3** 133–42
[5] Lippmann G 1908 Epreuves reversibles, photographies integrales *C. R. Acad. Sci., Paris* **146** 446–51
[6] Hutley M C and Stevens R F 1991 *The Formation of Integral Images by Afocal Pairs of Lens Arrays ('Superlenses')* (*IOP Short Meeting Series* 30) (Bristol: IOP Publishing) pp 147–54
[7] Daly D, Stevens R F, Hutley M C and Davies N 1990 The manufacture of microlenses by melting photoresist *Meas. Sci. Technol.* **1** 759–66
[8] Völkel R, Herzig H P, Nussbaum P, Dändliker R and Hugle W 1996 Microlens array imaging system for photolithography *Opt. Engng, Bellingham* **35** 3323–30
[9] Araki K 1990 Compound eye systems for nonunity magnification projection *Appl. Opt.* **29** 4098–104